mining

MDPI

Article

Temporal-Spatial Evolution of Acoustic Emission in Raw Coal with Pre-Fabricated Roadway: An Experimental Study for Mining Geomechanics

Xugang Fang [1], Yunpeng Zhang [2,*], Sizhan Sun [1], Shijian Zhang [1], Zhengcheng Li [1], Yongxiang Li [1], Qi Ma [3,4,*], Chengtao Xin [2], Chaolan Zhou [2] and Weizhi Diao [2]

[1] Yunnan Chihong Zinc-Germanium Co., Ltd., Qujing 655011, China; xugang_fang@chinalco.com.cn (X.F.); sizan_sun@chinalco.com.cn (S.S.); sj_zhang@chinalco.com.cn (S.Z.); lizhengcheng@chinalco.com.cn (Z.L.)
[2] Kunming Metallurgical Research Institute Co., Ltd., Kunming 650031, China
[3] School of Safety Engineering, North China Institute of Science and Technology, Langfang 065000, China
[4] School of Safety Engineering, China University of Mining and Technology, Xuzhou 221116, China
* Correspondence: 15025188685@126.com (Y.Z.); cumtckgc@163.com (Q.M.)

Abstract

Roadway surrounding rock stability under high in-situ stress is a core challenge in mining geomechanics. This paper presents an empirical and analytical study on the temporal-spatial evolution of acoustic emission (AE) during fracture of raw coal specimens with a pre-fabricated simulated roadway. A true triaxial loading system was adopted to reproduce two typical stress paths, i.e., vertical loading coupled with lateral unloading and pure vertical loading, to mimic the stress redistribution characteristics induced by deep roadway excavation and subsequent mining disturbance. AE event counts, time-frequency features, 3D source locations and energy distributions were synchronously acquired via a 24-channel monitoring system. Results show that notable stress concentration zones form around the pre-fabricated roadway under both stress paths, while the instability modes present significant differences. Under the vertical loading coupled with lateral unloading path, macroscopic instability lags over 150 s behind the AE activity peak, exhibiting clear precursor characteristics. In contrast, under the pure vertical loading path, local abrupt instability occurs without obvious abrupt change in AE event counts, showing typical sudden brittle fracture characteristics. Prior to failure, AE energy and amplitude fluctuate sharply and the dominant frequency shifts to high-frequency bands, serving as quantitative indicators for accelerated fracture. Fractures initiate from the borehole wall and expand radially; high-energy AE zones align well with major fracture paths. These findings provide experimental support for fracture early warning and surrounding rock stability evaluation in deep coal roadways, and offer reference for mining geomechanical design and ground support optimization.

Keywords: pre-fabricated roadway; raw coal; true triaxial test; acoustic emission; temporal-spatial evolution; mining geomechanics; roadway stability

Check for updates

Academic Editor: Ali Mirzaghorbanali

Received: 14 September 2026
Revised: 6 October 2026
Accepted: 7 October 2026
Published: 15 October 2026

Copyright: © 2026 by the authors. Licensee MDPI, Basel, Switzerland. This article is an open access article distributed under the terms and conditions of the Creative Commons Attribution (CC BY) license.

1. Introduction

The stability of underground roadways is a fundamental issue in mining geomechanics and a core prerequisite for safe and efficient deep coal mining. As coal mining progresses to greater depths, surrounding rock masses are subjected to high in-situ stress, strong mining disturbance, and heterogeneous stress fields, where the initiation, propagation and

coalescence of micro-fractures can easily trigger dynamic disasters such as roof falls, rib spalling and rock bursts [1,2]. Empirical laboratory testing, analytical characterization, and numerical simulation constitute the three mainstream approaches for investigating rock mass failure mechanisms and supporting geomechanical design in mining engineering. Acoustic emission (AE) technology, as a typical experimental and analytical tool, enables real-time capture of elastic wave signals induced by internal micro-fracture evolution, and has become a core technique for roadway stability monitoring and disaster early warning [3,4]. However, the temporal-spatial evolution laws of AE in raw coal (raw coal specimen) containing pre-fabricated roadways under the coupled stress path of vertical loading and lateral unloading remain insufficiently understood, which limits the accurate identification of excavation-induced damage mechanisms and the application of targeted early warning strategies [5,6].

True-triaxial loading tests can realistically reproduce the underground triaxial unequal stress state. As a mainstream experimental approach for investigating the mechanical behavior and fracture mechanism of coal-rock masses, it has been widely employed to study mechanical properties such as triaxial compression, unloading disturbance, and cyclic loading-unloading for rock masses of coal, sandstone and limestone [7–9]. Taking advantages of multi-parameter characterization, three-dimensional localization and visual analysis, acoustic emission technology enables quantitative tracking of the whole disaster evolution process of coal-rock masses. Relevant research achievements have been successfully applied to monitoring and early-warning for scenarios including tunnel rockburst, ground pressure in metal mines, and roadway surrounding rock fracture [10–13]. With the advancement of intelligent mine construction, technologies such as advance detection of driving face, intelligent tunneling equipment, machine-vision recognition and three-dimensional reconstruction have achieved rapid development, which greatly improves the intelligence level of roadway construction and surrounding rock monitoring [14,15].

In recent years, numerous scholars have conducted extensive research on the acoustic emission response laws of rock masses under complex stress paths. Studies including rock-mass disaster characteristics under true-triaxial cyclic loading-unloading, mechanical behaviors of sandstone under true-triaxial unloading disturbance, and acoustic emission characteristics of deep limestone have continuously improved the theoretical system of rock-mass fracture and acoustic emission response under complex stress fields [16–18]. Research outputs such as rockburst simulation tests, overlying strata movement laws, inversion of mining-induced stress fields, and short-term rockburst prediction have provided important references for the monitoring and early warning of mine dynamic disasters [19–23]. Meanwhile, the effects of factors including water content, bedding property, high temperature and pre-fabricated defects on the mechanical and acoustic emission characteristics of rock masses have been systematically revealed, which further enriches the disaster mechanics and acoustic emission theories for coal-rock masses [24,25]. Microseismic monitoring technology has also been widely adopted in ground-pressure control projects such as caving method, filling method and coordinated mining, promoting the technical upgrading of mine safety prevention and control [26–28].

Although abundant achievements have been obtained in existing studies, obvious deficiencies still remain. Most researches focus on intact coal-rock masses, conventional sandstone and limestone. Systematic experimental investigations on raw coal with pre-fabricated simulated roadways concerning acoustic emission temporal characteristics, time-frequency evolution laws and spatial localization distribution under the coupled stress path of vertical loading-lateral unloading are relatively scarce. Accordingly, it is difficult to accurately reveal the internal mechanisms of stress concentration around openings, radial fracture propagation and concentrated energy release induced by roadway excavation

disturbance, which fails to meet the on-site requirements for precise monitoring, advance early warning and dynamic support.

To address this research gap, this paper conducts an empirical and analytical study on raw coal specimens containing pre-fabricated simulated roadways within the scope of mining geomechanics. A true triaxial loading system is adopted to reproduce the coupled stress path of vertical loading combined with lateral unloading, which replicates the stress redistribution induced by deep roadway excavation. A 24-channel acoustic emission monitoring system is applied to synchronously capture AE event counts, time-frequency features, three-dimensional source locations, and energy nephograms throughout the whole fracture process. The temporal-spatial evolution laws of AE during coal-rock failure are systematically analyzed, and the control mechanisms of the roadway structure and loading-unloading path on fracture patterns are clarified. A multi-parameter AE-based method for surrounding rock damage identification and precursor early warning is further proposed. Most existing studies take intact coal-rock specimens as research objects, while this study adopts raw coal specimens with pre-fabricated simulated roadways, which can realistically reproduce the stress concentration effect and fracture initiation characteristics around excavated openings. Most existing studies employ conventional monotonic loading or cyclic loading-unloading paths, while this study designs a stress path of vertical loading coupled with lateral unloading, which matches the mechanical characteristics of stress redistribution induced by deep roadway excavation. The findings can provide experimental basis and analytical support for roadway stability assessment, dynamic support optimization and geohazard mitigation in deep coal mines, and also offer a reference for empirical-analytical research on similar mining geomechanics problems.

2. Materials and Methods

2.1. Specimen Preparation and Experimental Apparatus

The test adopts the coal-rock dedicated true-triaxial loading apparatus independently developed by China University of Mining and Technology (Figure 1). The apparatus mainly consists of a loading frame, vertical and horizontal loading units, independent hydraulic pump stations, a triaxial pressure chamber, spacer blocks for acoustic-emission sensor installation, and a computer measurement-and-control system. Adopting electro-hydraulic servo control, the apparatus has a maximum vertical loading capacity of 1600 kN and a maximum horizontal loading capacity of 600 kN. Each loading unit in different directions can independently perform loading-unloading operations without mutual interference. Equipped with loading spacers of various sizes, the apparatus can conduct loading tests on cubic specimens with side lengths of 200 mm, 150 mm and 100 mm. In this test, 150 mm loading spacers were used to match the size of the prepared specimens. By simple program settings, multiple loading paths including continuous loading, stepwise loading and cyclic loading-unloading under uniaxial, biaxial and true-triaxial stress conditions can be realized. The loading rate control accuracy reaches 0.05 MPa/s, which can equivalently reproduce the in-situ stress adjustment rate of surrounding rock during deep roadway excavation. In the acoustic-emission monitoring system, a maximum of four sensors can be arranged on a single spacer block, and 24 sensors can perform synchronous acquisition during the test. Multi-channel synchronous monitoring greatly improves the spatial resolution and data integrity of acoustic-emission signals. Through optimized sensor layout, three-dimensional localization and dynamic tracking of internal acoustic-emission sources within specimens can be achieved. The temporal-spatial evolution laws of acoustic emission from stress-induced damage to overall fracture of raw coal can be fully obtained, which provides accurate and detailed data support for revealing the evolutionary mechanism of fracture initiation, propagation, coalescence and eventual macroscopic instability.

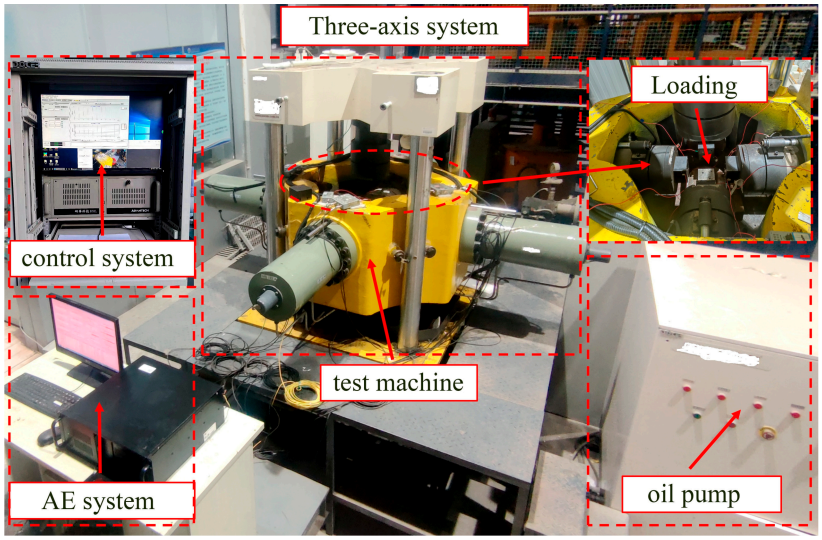
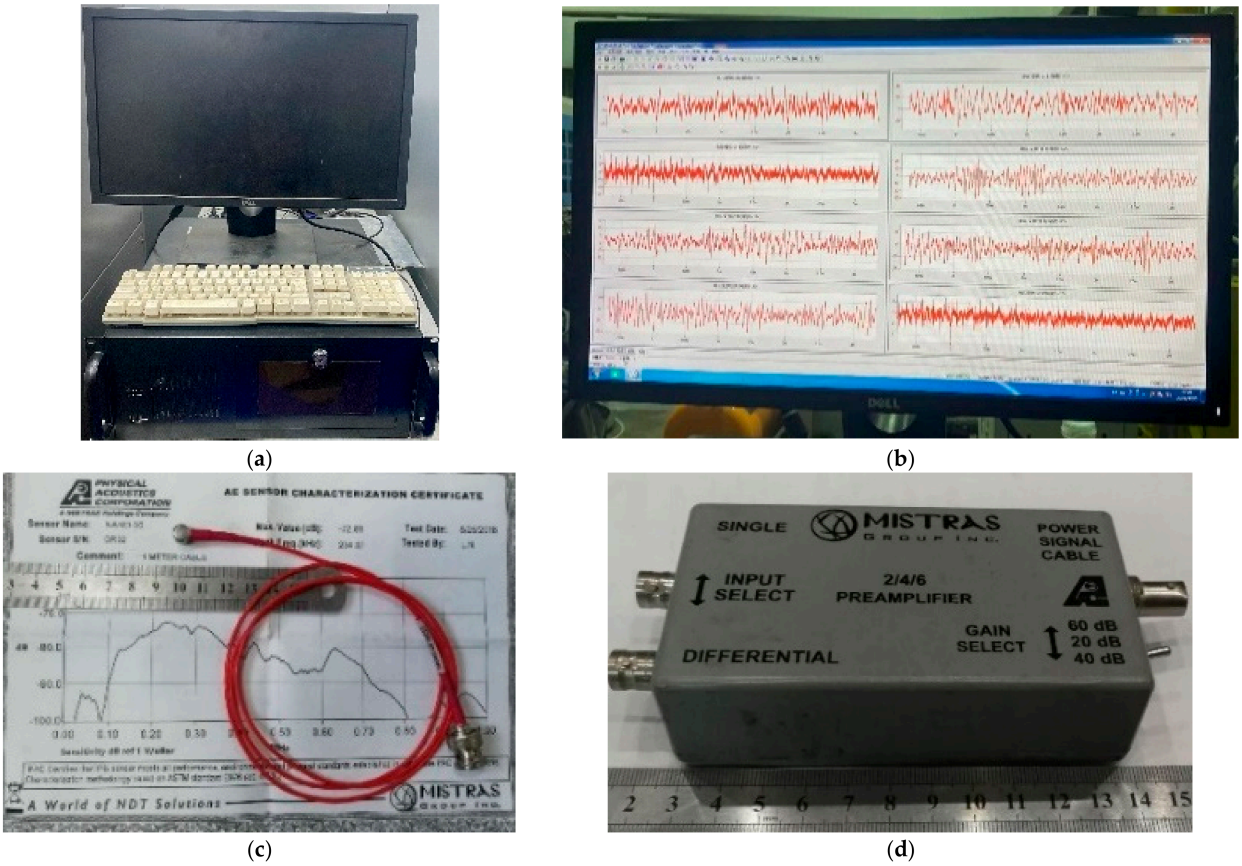


Figure 1. True Triaxial Loading System.

As shown in Figure 2, the acoustic emission monitoring system adopted in this test is mainly composed of a hardware acquisition unit and supporting analysis software. The hardware mainly includes an acoustic emission main acquisition unit, preamplifiers and sensors, and the supporting processing software is AEwin (Version 2.0, Physical Acoustics Corporation, Princeton Junction, NJ, USA) developed by Physical Acoustics Corporation (PAC), MISTRAS Group, Inc., Princeton Junction, NJ, USA. The acquisition equipment used in the test is the Micro-II type acquisition instrument of this company, which is equipped with three PCI-8 acquisition cards and provides 24 data acquisition channels. The gain of the preamplifier is set to 40 dB. As signal-sensing elements in direct contact with coal-rock specimens, the performance of sensors directly determines the quality of acquired signals. Considering test conditions such as specimen size, Nano30 acoustic emission sensors are finally selected. With a probe diameter of only 8 mm, this sensor can not only efficiently receive acoustic emission signals on the specimen surface, but also minimize interference to the internal stress field and mechanical response of the specimen. Its operating frequency band ranges from 125 kHz to 750 kHz, which fully covers the main effective signal frequency range during the loading-induced damage and fracture of raw coal, and provides reliable support for accurately analyzing the internal damage evolution law of raw coal. A total of 8 Nano30 sensors were arranged on the specimen surface in this test. Custom-sized acrylic plates (147 mm × 147 mm) were adopted for sensor installation and fixation: first, the acrylic plates were bonded to the preset positions on the specimen surface with double-sided adhesive tape; then the Nano30 sensors were embedded into the pre-drilled holes of the acrylic plates, with black rubber spacers and plasticine sequentially laid on the outer side of the sensors. This design ensures effective acoustic signal coupling, and uniformly transfers the confining pressure load to the sensors, while effectively avoiding mutual extrusion between adjacent plates under triaxial loading. The AE system sampling frequency was set to 2 MSPS with continuous acquisition throughout the whole test. The noise threshold was set to 45 dB to effectively filter interferences from the loading frame, hydraulic system and environmental electromagnetic noise. Before the formal test, pencil-break tests were carried out to calibrate sensor coupling conditions and system wave velocity, ensuring that the three-dimensional location error of AE sources was less than 2 mm.

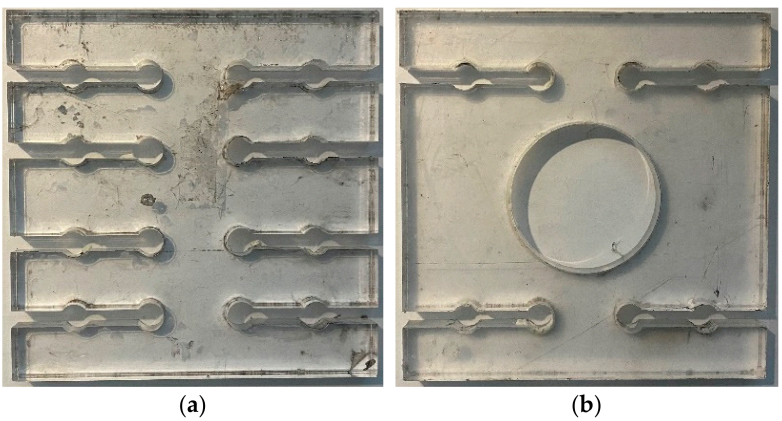


(**a**) (**b**)

(**c**) (**d**)

Figure 2. Acoustic Emission Monitoring System: (**a**) Acoustic emission acquisition instrument; (**b**) AEwin software. (**c**) Acoustic emission sensor; (**d**) Preamplifier.

In the test, acrylic plates (Figure 3) were used to position and fix the Nano30 sensors (Figure 4), and the detailed dimensional parameters are shown in Figure 5. The specific assembly procedure is as follows. First, special-purpose acrylic plates are machined according to the sensor layout scheme and bonded onto the specimen surface with double-sided adhesive tape. Then the Nano30 sensors are embedded into the pre-drilled holes of the acrylic plates. Black rubber spacers and plasticine are sequentially placed on the outer side of the sensors. Confining pressure load is uniformly transferred to the sensors through these two components. The acrylic plates adopted in this test are sized 147 mm × 147 mm. Verified by tests, this dimension can effectively avoid mutual extrusion between adjacent plates that occurs for standard 150 mm × 150 mm plates under triaxial loading.



(**a**) (**b**)

Figure 3. Physical object of acrylic plate: (**a**) acrylic plate-2; (**b**) acrylic plate-2.

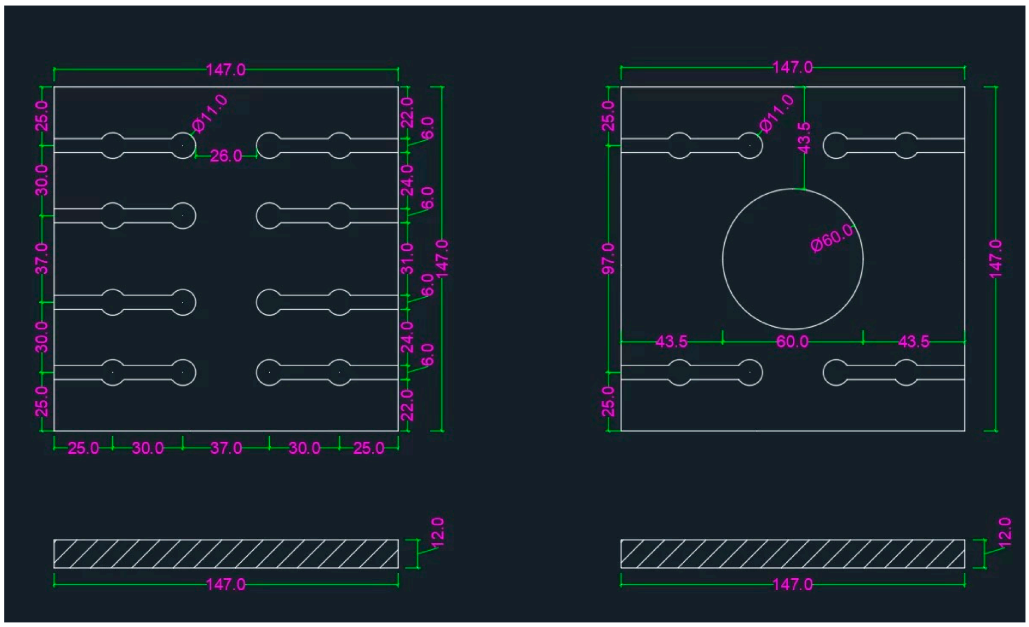


Figure 4. Dimensions of Acrylic Plate.

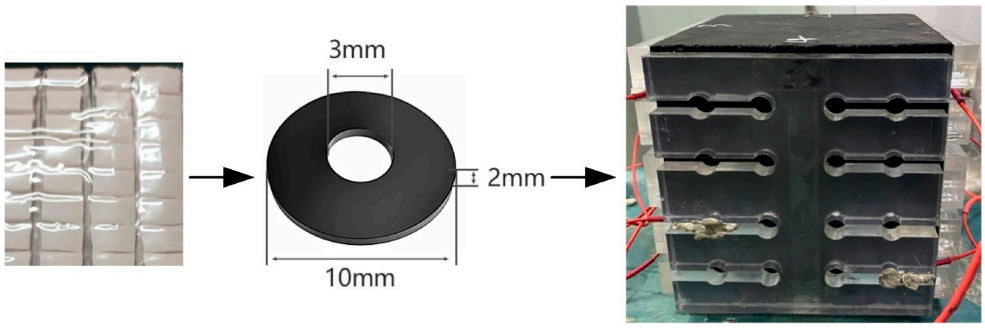


Figure 5. Schematic Diagram of Nano30 Sensor Installation.

The uniaxial compressive strength of the raw coal specimens used in this test is approximately 14 MPa. To adapt to diverse test conditions, raw coal blocks were machined into cubic specimens of 150 mm × 150 mm × 150 mm in accordance with the suggested standards of the International Society for Rock Mechanics (ISRM). All specimens were prepared strictly in compliance with specifications, with dimensional deviation controlled within ±0.2 mm and end-face flatness not exceeding 0.05 mm. After fine grinding, the specimens exhibited uniform and compact texture with smooth surfaces, and no obvious primary joints or fractures were observed. The homogeneity of specimens was comprehensively evaluated by measuring specimen density and acoustic wave velocity. Specimens with similar physico-mechanical parameters (No. ZM-1) were preferentially selected for the test to guarantee favorable stability and comparability of test data.

All eligible specimens (six) were divided into two groups matching the two designed stress paths: one for the vertical loading coupled with lateral unloading test, and the other for the pure vertical loading test. One representative specimen with optimal homogeneity was selected from each group for detailed analysis.

To obtain a regular configuration of the pre-fabricated simulated roadway with high similarity to practical engineering, numerically-controlled high-precision drilling equipment was adopted for specimen preparation. The drilling axis was strictly perpendicular to the top surface of the specimen, and the hole wall was smooth without debris or additional damage, so as to prevent artificial defects from interfering with test results. After machining, specimens were kept static for 24 h to eliminate residual stress induced by mechanical

processing. Ultrasonic velocity and density were re-measured to ensure that the difference in physico-mechanical parameters among groups was controlled within 5%.

Raw coal (Figure 6) is characterized by well-developed internal micro-pores, weak planes and bedding planes, which lead to remarkable heterogeneity in stress transfer under triaxial stress. The existence of the pre-fabricated roadway further alters the stress distribution pattern, rendering the area around the opening the preferred zone for fracture initiation and propagation. Standardized specimen preparation, homogeneity screening and precise loading control can minimize test dispersion, improve the reliability and repeatability of acoustic emission response laws, and make the test results better reflect the real fracture behavior of surrounding rock in deep roadways.

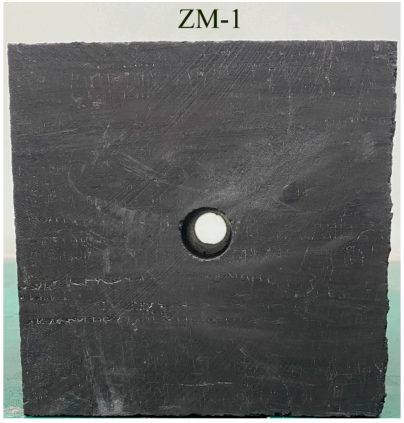


Figure 6. Raw coal specimen.

2.2. Stress-Path Design and Acoustic-Emission Monitoring Scheme

A total of eight Nano-30 acoustic emission sensors were deployed in this test to realize location monitoring of acoustic emission sources. The detailed spatial layout scheme of each sensor is shown in Table 1.

Table 1. Spatial Layout and Coordinates of Acoustic Emission Sensors.

Sensor No.	Coordinates (mm)			Sensor No.	Coordinates (mm)		
	X	Y	Z		X	Y	Z
N1	123.5	0	123.5	N5	93.5	147	93.5
N2	123.5	0	26.5	N6	123.5	147	23.5
N3	26.5	0	56.5	N7	23.5	147	123.5
N4	0	23.5	123.5	N8	0	123.5	23.5

Roadway excavation disturbs the initial stress field of surrounding rock, transforming it from a hydrostatic stress state into a non-isotropic triaxial stress state characterized by vertical loading and lateral unloading. Based on this mechanical characteristic, a multi-stage combined loading path of axial pressure and confining pressure under true-triaxial conditions was designed in this paper (Figure 7).

Pre-loading was first applied to the raw coal specimen with a pre-fabricated roadway: the triaxial stresses were increased uniformly at 0.05 MPa/s up to 2 MPa and maintained for 200 s. In the formal loading stage, σ_1, σ_2 and σ_3 were synchronously raised to 6 MPa at the same rate, after which σ_3 was kept constant. Then σ_1 and σ_2 were increased to 8 MPa and σ_2 was fixed. Afterwards, σ_1 was loaded to 12 MPa and held for 300 s. Subsequently, σ_1 was continuously applied until specimen fracture; meanwhile, σ_3 was gradually unloaded to 0 MPa at a rate of 0.02 MPa/s.

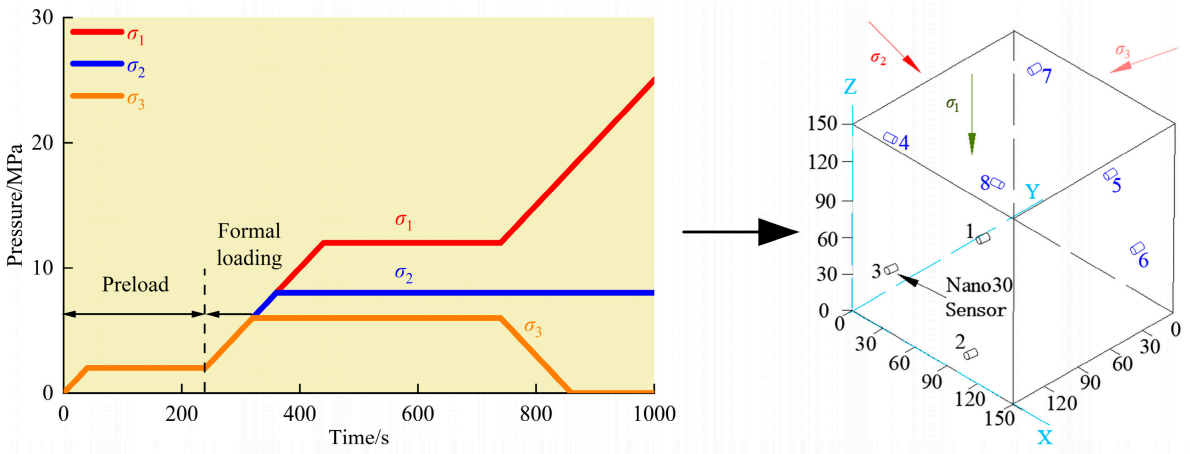


Figure 7. Test scheme of vertical loading-lateral unloading.

Acoustic emission location monitoring was adopted throughout the whole test, and the system sampling frequency was set to 2 MSPS. Acoustic emission threshold-triggered acquisition was used with a preamplifier gain of 40 dB and a sampling frequency of 2 MSPS to eliminate environmental and electromagnetic interference. A valid AE event was defined as a signal whose peak amplitude exceeded the 45 dB threshold and whose duration was longer than 1 μs, which further filtered out random electromagnetic noise and low-amplitude mechanical vibration interference. Before the test, pencil-break tests were carried out to calibrate sensor coupling conditions and system wave velocity, ensuring that the 3D location error was less than 2 mm. The pencil-break tests were performed at 5 preset positions on the specimen surface (four corners and the center of the top surface), with each position repeated 3 times. The three-dimensional location of AE sources was calculated using the time difference of arrival (TDOA) method based on the calibrated P-wave velocity. The loading rates were derived from the in-situ stress adjustment rate of surrounding rock during roadway excavation via equivalent conversion based on rock mechanics similarity criteria. Specifically, the engineering-scale stress evolution rate was scaled to the loading rate of laboratory specimens according to the geometric and temporal similarity ratios, which ensures both the operability of laboratory tests and the mechanical equivalence with the in-situ stress response.

Through the complete procedures of pre-loading, stepwise loading, stress holding, lateral unloading and continuous acquisition, the temporal, time-frequency and spatial evolution information of acoustic emission for raw coal covering the whole process from compaction-closure, elastic deformation, damage propagation to macroscopic instability can be comprehensively captured. It provides complete data support for revealing the damage mechanism under loading-unloading paths.

Stress, time, full-waveform acoustic emission signals and location data were recorded synchronously during the test. All data streams were aligned to a unified time axis to ensure accurate temporal correspondence between mechanical parameters and AE signals. For each valid AE event, the AE energy was calculated by integrating the square of the signal amplitude over time; the dominant frequency and secondary frequency were extracted via fast Fourier transform (FFT) of the full waveform. The noise threshold was set to 45 dB to effectively filter interferences from the loading frame, hydraulic system and environmental electromagnetic noise, ensuring that the collected signals originate from real fractures inside the coal-rock mass. The acoustic-emission wave velocity was calibrated based on the ultrasonic test results of specimens, so that the three-dimensional spatial location error was controlled within 2 mm. Multi-stage stepwise loading and synchronous lateral unloading were adopted to completely reproduce the dynamic stress adjustment

process of surrounding rock after deep roadway excavation, and the test stress path is highly consistent with the mechanical state of field engineering.

After the completion of roadway excavation construction, the surrounding rock behind the working face originally tends to be stable. Nevertheless, under subsequent mining disturbance, additional loads are imposed again in the vertical direction, which further induces local stress concentration and aggravates the damage and fracture of surrounding rock. Based on this engineering feature, combined working conditions with different axial pressures and confining pressures under true-triaxial conditions are designed in this paper, as illustrated in Figure 8.

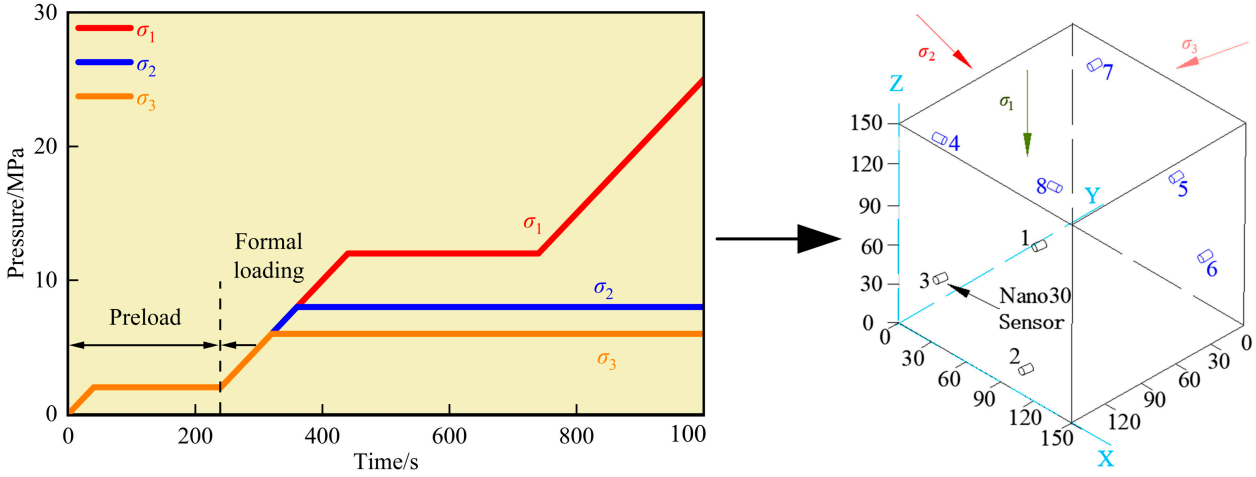


Figure 8. Vertical Loading Test Scheme.

Pre-compression treatment was firstly performed on the coal-rock specimen containing a pre-fabricated simulated roadway: the triaxial stresses were synchronously and uniformly applied up to 2 MPa at a rate of 0.05 MPa/s and held for 200 s. Upon entering the formal loading stage, the vertical principal stress σ_1 and two lateral stresses σ_2, σ_3 were further synchronously increased to 6 MPa at the same rate of 0.05 MPa/s, after which σ_3 was kept constant until the termination of the test. Afterwards, σ_1 and σ_2 were continuously raised to 8 MPa at the identical rate, and σ_2 was maintained unchanged. Subsequently, σ_1 was loaded to 12 MPa at 0.05 MPa/s and held for 300 s. Then σ_1 was continuously loaded at this rate until complete instability and fracture of the specimen. Acoustic emission location monitoring was carried out synchronously throughout the test, and the system sampling frequency was set to 2 MSPS.

Stress time curves and full waveform acoustic emission data were synchronously acquired throughout the test. The threshold triggered mode was adopted to collect valid signals so as to eliminate electromagnetic interference and mechanical noise. To guarantee location accuracy, sensor coupling performance, wave velocity parameters and system attenuation characteristics were calibrated before the test, and pencil break tests were used for effectiveness verification. The loading rate was obtained through equivalent conversion of the in-situ stress adjustment rate of surrounding rock during roadway excavation based on rock mechanics similarity criteria. The engineering-scale stress evolution rate was scaled to match the size of laboratory specimens, so as to reproduce the real stress evolution rhythm of underground surrounding rock while ensuring test operability. Via multi stage stress holding, stepwise loading and continuous acquisition, the acoustic emission response information of raw coal throughout the whole process from compaction, elastic deformation, damage propagation to local instability was fully captured. The loading rates, holding times and final stress values of all stages for the two groups of tests are summarized in Table 2.

Table 2. Summary of loading parameters for two groups of true triaxial tests.

Test Group	Loading Stage	Loading Rate (MPa/s)	Holding Time (s)	Stress at the End of Stage ($\sigma_1/\sigma_2/\sigma_3$, MPa)
Group 1: Vertical loading coupled with lateral unloading test	Pre-loading stage	0.05	200	2/2/2
	Isotropic loading stage (2 → 6 MPa)	0.05	-	6/6/6
	Anisotropic loading stage (6 → 8 MPa)	0.05	-	8/8/6
	Principal stress loading stage (8 → 12 MPa)	0.05	300	12/8/6
	Confining pressure unloading & fracture loading stage	0.05 (σ_1)/0.02 (σ_3)	-	25/8/0
Group 2: Pure vertical loading test	Pre-loading stage	0.05	200	2/2/2
	Isotropic loading stage (2 → 6 MPa)	0.05	-	6/6/6
	Anisotropic loading stage (6 → 8 MPa)	0.05	-	8/8/6
	Principal stress loading stage (8 → 12 MPa)	0.05	300	12/8/6
	Axial loading stage until fracture	0.05 (σ_1)	-	35/8/6

3. Results

3.1. Temporal Evolution of Acoustic-Emission Activity Under Mining-Induced Stress Paths

In this study, vertical-loading and lateral-unloading tests were performed on raw coal specimens with pre-fabricated boreholes according to the stress application characteristics. The test procedure was systematically divided into two stages: pre-loading and formal loading. During the test, event identification and analysis were conducted on the collected acoustic emission signals to obtain the generation quantity of acoustic-emission event waveforms per unit time. The stress variation law of the raw coal specimen throughout the test and the evolution characteristics of acoustic-emission event waveform counting over time are presented in Figure 9.

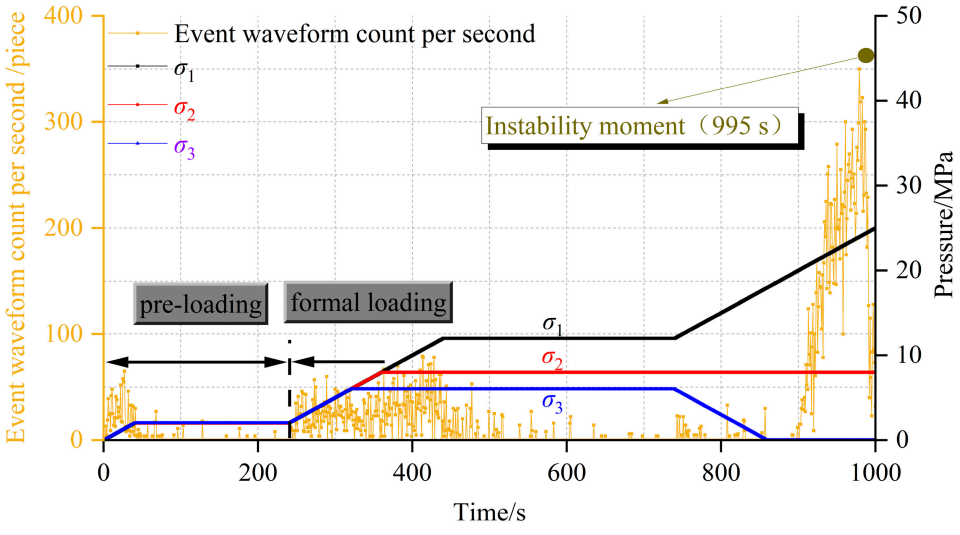


Figure 9. Acoustic-Emission Event Waveform Counting Induced by Raw Coal Fracture Under Loading-Unloading Conditions.

The test results show that the instability and fracture of the raw coal specimen occur in the late stage of the test, and the instability time is obviously later than the moment when the acoustic-emission event waveform counting reaches its peak. The phenomenon that the instability moment lags behind the AE peak indicates that there exists a period of accelerated damage propagation after the stress peak for raw coal. Acoustic emission can reflect fracture precursors more than 150 s in advance, exhibiting remarkable early-warning capability. Vertical loading raises the stress level of surrounding rock, while lateral unloading weakens confining pressure constraint. Their coupling promotes rapid propagation and coalescence of fractures. The pre-fabricated roadway aggravates stress concentration, and acoustic-emission active points emerge earlier and distribute more intensively, demonstrating that the opening structure acts as a key factor controlling fracture initiation and development. Such precursors can hardly be identified merely by stress monitoring, whereas acoustic-emission event counting can serve as a core indicator for early damage identification and stability discrimination.

The peak value of acoustic emission occurs prior to macroscopic instability, which is a direct reflection of massive initiation and propagation of micro-cracks inside coal-rock mass. It also indicates that acoustic emission can identify the accelerated damage development stage before macroscopic fracture takes place. Vertical loading provides the driving force for fracture propagation, while lateral unloading weakens the constraint effect of confining pressure. Their coupling significantly accelerates the coalescence rate of fractures. The pre-fabricated roadway structure remarkably enhances the stress-concentration effect, leading to earlier initiation and faster development of fracture. Such precursor information can hardly be captured merely by stress monitoring, which further demonstrates the unique advantages of acoustic-emission technology in early-damage identification.

In this study, vertical-loading tests were carried out on raw coal specimens with pre-fabricated boreholes. The whole test process was divided into pre-loading and formal loading according to different stress-application stages. During the test, event discrimination was performed on the collected acoustic-emission signals, and the number of acoustic-emission event waveforms per unit time was statistically counted. The evolution curves of applied loading stress and acoustic-emission event waveform counting of raw coal with time are shown in Figure 10.

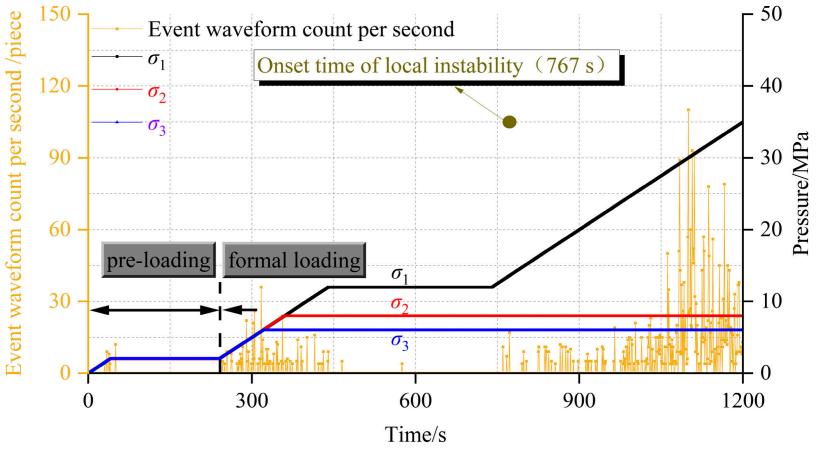


Figure 10. Acoustic-Emission Event Waveform Counting Induced by Raw Coal Fracture Under Loading Conditions.

The test results reveal that the overall instability of the raw coal specimen does not occur in the late loading stage; instead, fracture takes place at 767 s of the test. This is because the pre-fabricated simulated roadway forms a stress-concentration zone inside the specimen. Under loading, the stress in this zone first reaches the bearing limit of coal-rock

mass, thereby inducing local instability and fracture. Notably, specimen instability occurs at the initial loading stage after stress holding, while no obvious abrupt change is observed in acoustic-emission event waveform counting at this moment. It indicates that instantaneous loading is the dominant inducement triggering the fracture of raw coal specimens.

3.2. Time-Frequency Characteristics of Acoustic Emission During Coal-Rock Fracture Evolution

Figure 11 illustrates the variation trends of the average values of various time-frequency parameters of acoustic-emission event waveforms per unit time during raw coal fracture under the combined effect of vertical loading and lateral unloading. The test results show that obvious abnormal fluctuations occur in the root-mean-square amplitude energy per second and the rectified average value within the critical stage of 150 s prior to raw coal instability, which reflects the continuous adjustment of the internal stress field of rock mass and the rising intensity of fracture activities. The mean values of dominant frequency and secondary frequency oscillate violently in multiple frequency bands, and the proportion of high-frequency components increases substantially, presenting an overall abnormal feature of high-level oscillation. This phenomenon indicates that the initiation, propagation and interaction of fractures with different scales inside coal-rock mass are significantly intensified, which implies that instability and fracture of rock mass are forthcoming.

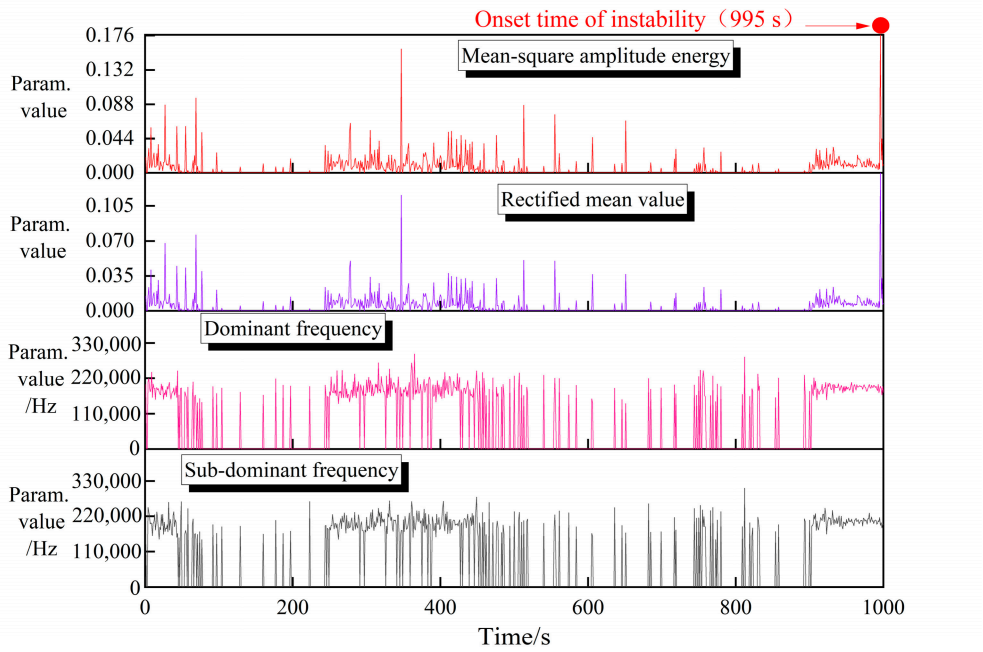


Figure 11. Average Values of Time-Frequency Characteristics of Acoustic-Emission Event Waveforms per Second during Raw Coal Fracture under Loading-Unloading Conditions.

A remarkable rise in high-frequency components implies a substantial increase in micro-fracture density, which serves as a typical precursor before fracture coalescence. The anomalies of root-mean-square amplitude energy and dominant frequency can be adopted as critical early-warning thresholds for field monitoring. When the energy fluctuates and rises continuously and the dominant frequency shifts toward the high-frequency band, it indicates that the surrounding rock around the opening has entered an accelerated fracture stage, and reinforcement support measures should be implemented in a timely manner. The temporal precursor law revealed by the test is free from the influence of macroscopic deformation lag and possesses higher sensitivity. It can provide quantitative references for advance early warning, dynamic support adjustment and risk hierarchical management at

underground roadway excavation working faces, and is of great value for improving the multi-parameter early-warning system of coal-rock dynamic disasters.

Figure 12 presents the average evolution laws of four time-frequency indicators (root-mean-square amplitude energy, rectified average value, dominant frequency and secondary frequency) of acoustic-emission event waveforms per unit time throughout the raw-coal fracture process under the vertical-loading condition. Among them, the peak occurrence time of root-mean-square amplitude energy is highly consistent with the moment when coal-rock mass enters the critical instability state (local instability-fracture of raw coal occurs at 767 s).

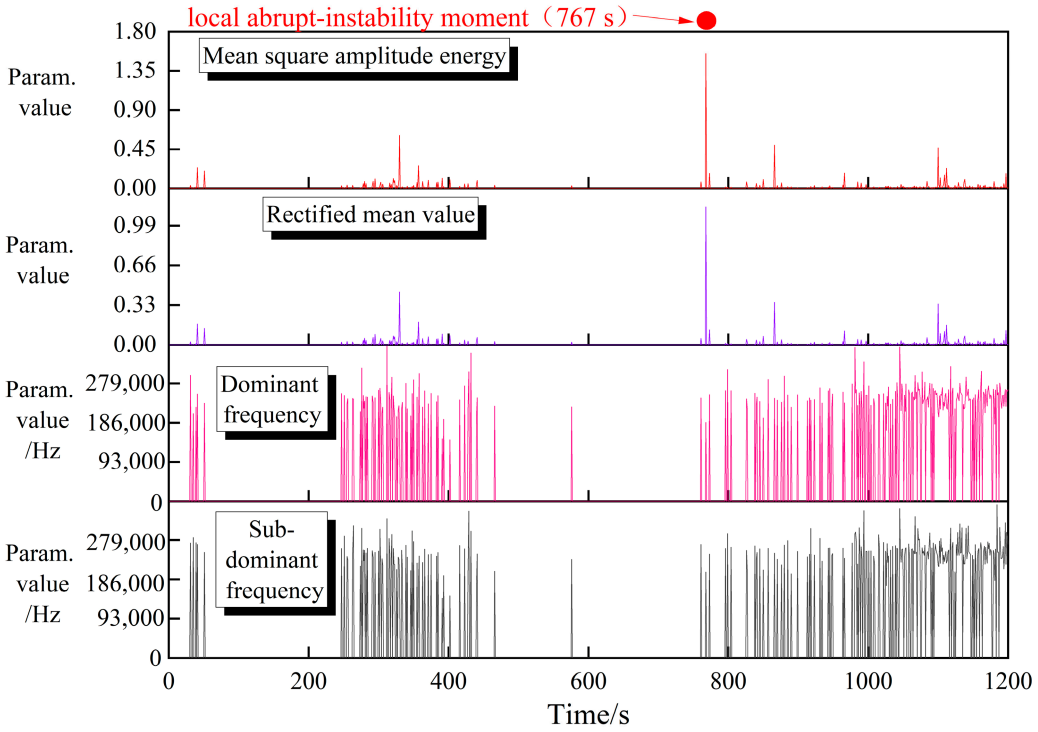


Figure 12. Average Values of Time-Frequency Characteristics of Acoustic-Emission Event Waveforms per Second during Raw Coal Fracture under Loading Conditions.

During the test, the triaxial confining pressures remained constant and no additional load was applied before local instability of raw coal. Nevertheless, local instability of coal-rock mass occurred rapidly after the abrupt increase of vertical stress. In-depth analysis shows that the abrupt change of stress field acts as the direct inducement for the rapid propagation of micro-cracks within the local stress-concentration zone. At the stage with constant triaxial confining pressures, the stress-concentration level of inherent weak structures (fractures, bedding planes, etc.) inside coal-rock mass is relatively low, and most micro-cracks are in the state of closure or low-speed propagation. At this moment, rock-mass deformation is dominated by elastic deformation, and the critical condition for high-speed crack propagation has not been satisfied.

The abrupt application of vertical principal stress σ_1 breaks the original stress equilibrium, resulting in a sharp rise in stress difference and vertical stress gradient, which exceeds the instantaneous bearing capacity of coal-rock mass. Accordingly, the stress state transforms from "quasi-static stability" to "dynamic instability". Under abrupt stress change, inherent defects inside coal-rock mass (fractures, pores, bedding planes, etc.) become the initiation points of stress concentration. Once micro-crack propagation is induced by a certain defect, redistribution of the surrounding stress field takes place, which further strengthens the stress-concentration effect of adjacent defects, namely the stress-shadow

effect. The high-stress zones of various defects superpose with one another and form local high-intensity stress belts, which promote chained coalescence and propagation of cracks and eventually trigger instability-fracture.

The staged-evolution characteristics of time-frequency parameters can serve as a quantitative basis for classifying the damage state of raw coal. In field monitoring, the continuous rise of root-mean-square amplitude energy and the shift of dominant frequency toward the high-frequency band can be regarded as identification markers for surrounding rock entering the accelerated-fracture stage. The time-frequency precursor law obtained from the test is immune to the hysteresis of macroscopic deformation and can reflect the internal fracture state at an earlier time. It can provide more sensitive judgment references for advance early-warning and dynamic support decision-making at roadway excavation working faces, and possesses important reference value for improving the multi-parameter joint early-warning system of surrounding rock in coal roadways.

3.3. Spatial Distribution of Acoustic-Emission Events and Fracture Localization

Roadway excavation operation induces strong artificial disturbance to surrounding rock and further triggers the readjustment of surrounding-rock stress field. Therefore, it is of great engineering significance to investigate the damage and fracture characteristics of coal-rock mass under the coupling effect of loading-unloading and excavation.

For the calculation of root-mean-square amplitude energy nephogram, the root-mean-square amplitude energy of acoustic-emission event waveforms generated by coal-rock fracture is firstly calculated. Afterwards, the peak values of two key indicators from each event waveform are extracted. Then, spatial nephograms are plotted by combining Gaussian spatial smoothing and Kriging interpolation methods. The specific implementation procedures are as follows: the research space is meshed with step size s. Taking each grid node as the center and r as the sliding statistical radius, the root-mean-square amplitude energy of microseismic event waveforms within this scope is accumulated and counted. In practical calculation, the radius r is generally set equal to the microseismic location error (2 mm). The grid size s satisfies the constraint of $s \leq r$ and takes a corresponding millimeter-scale value. Based on the event frequency and cumulative energy results within each grid cell, the root-mean-square amplitude energy nephogram of acoustic-emission event waveforms is finally generated after spatial interpolation.

Figures 13–15 sequentially present the macroscopic fracture morphology, acoustic-emission spatial-location results and root-mean-square amplitude energy nephograms of raw coal specimens under vertical-loading-lateral-unloading conditions. Figure 16 shows the synchronously acquired borehole endoscopic images. The experimental observations reveal that fractures all initiate from the borehole wall and expand outwards in a radial pattern, and the overall morphology of fractures is relatively regular.

The initiation and propagation of fractures are always accompanied by high level energy release. High energy accumulation zones are usually the locations where fractures initiate and propagate rapidly. The continuous extension of fractures will in turn further aggravate energy release, forming a mutually promoted chained response between them.

Fracture morphologies on different observation surfaces of the two types of specimens exhibit obvious diversity, and they are spatially connected and mutually coalesced, eventually forming a three dimensional fracture network that induces overall instability fracture of rock mass. The distribution of fractures on each surface of rock specimens is non uniform, and notable differences exist in fracture quantity and propagation characteristics among different surfaces.

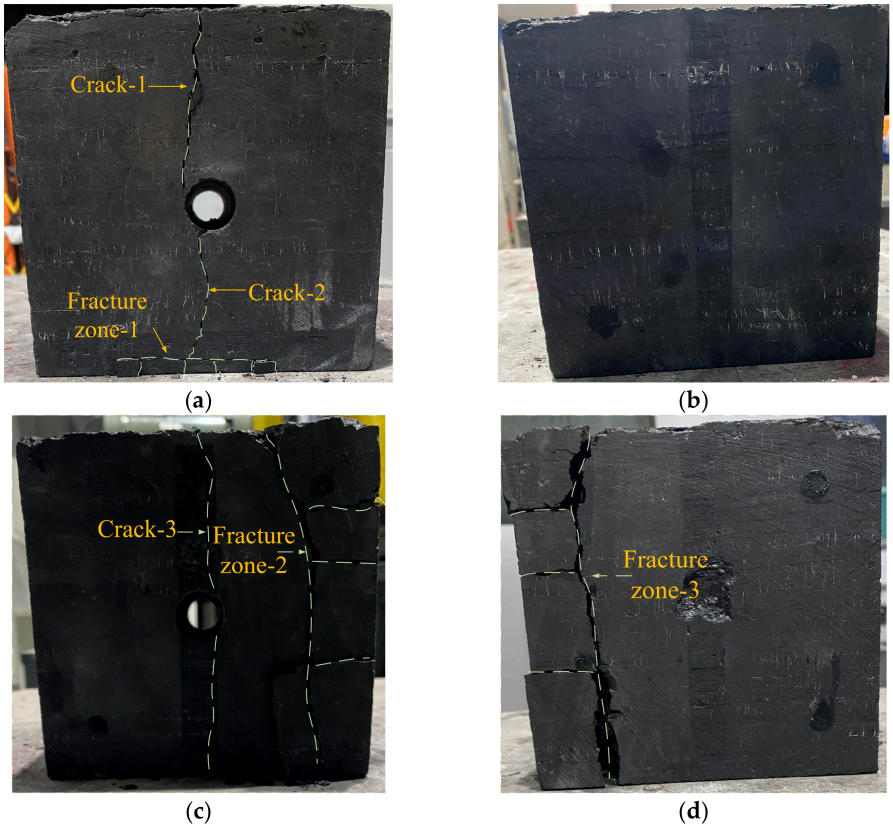


Figure 13. Macroscopic Fracture Appearance of Raw Coal under Loading-Unloading Conditions: (**a**) Front view; (**b**) Right side view; (**c**) Rear view; (**d**) Left side view.

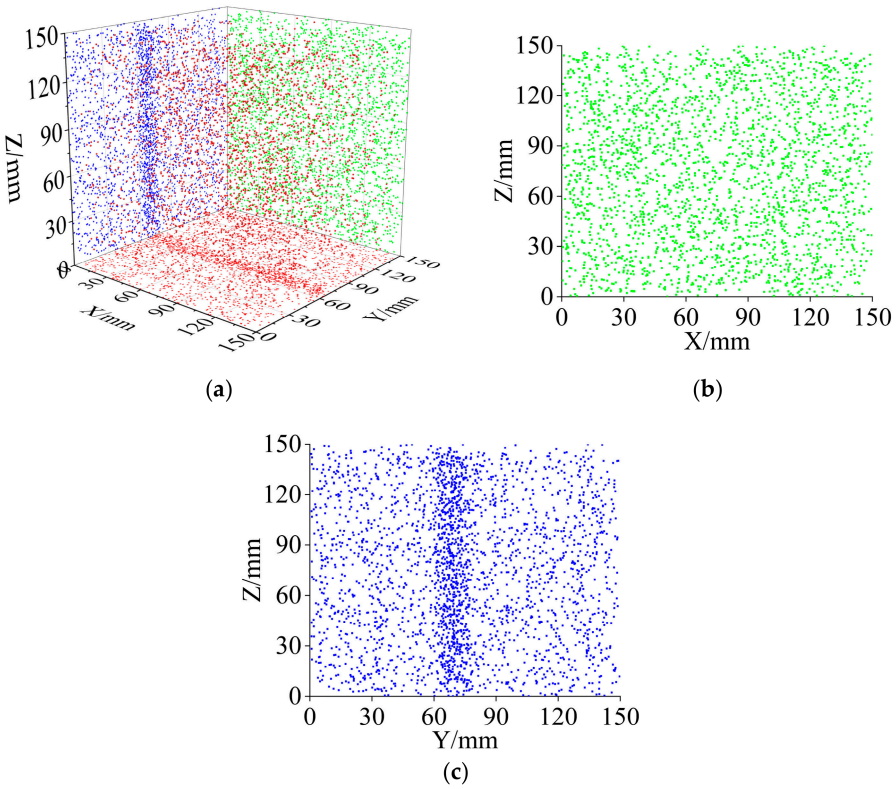


Figure 14. Location Results of Acoustic Emission Events during Raw Coal Fracture under Loading-Unloading Conditions: (**a**) 3 D Acoustic Emission Location; (**b**) Location Projection on XZ Plane; (**c**) Location Projection on YZ Plane.

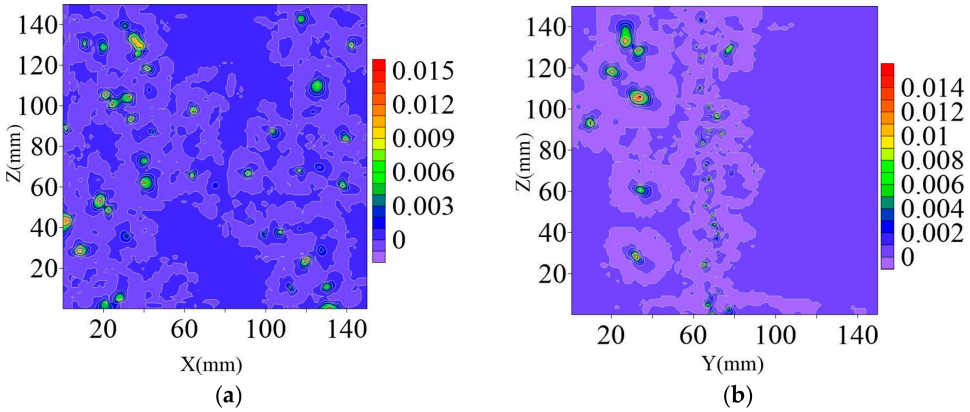


Figure 15. Acoustic Emission Nephograms of Raw Coal Fracture under Loading-Unloading Conditions: (**a**) Root Mean Square Amplitude Energy Nephogram of Event Waveforms on XZ Plane; (**b**) Root Mean Square Amplitude Energy Nephogram of Event Waveforms on YZ Plane.

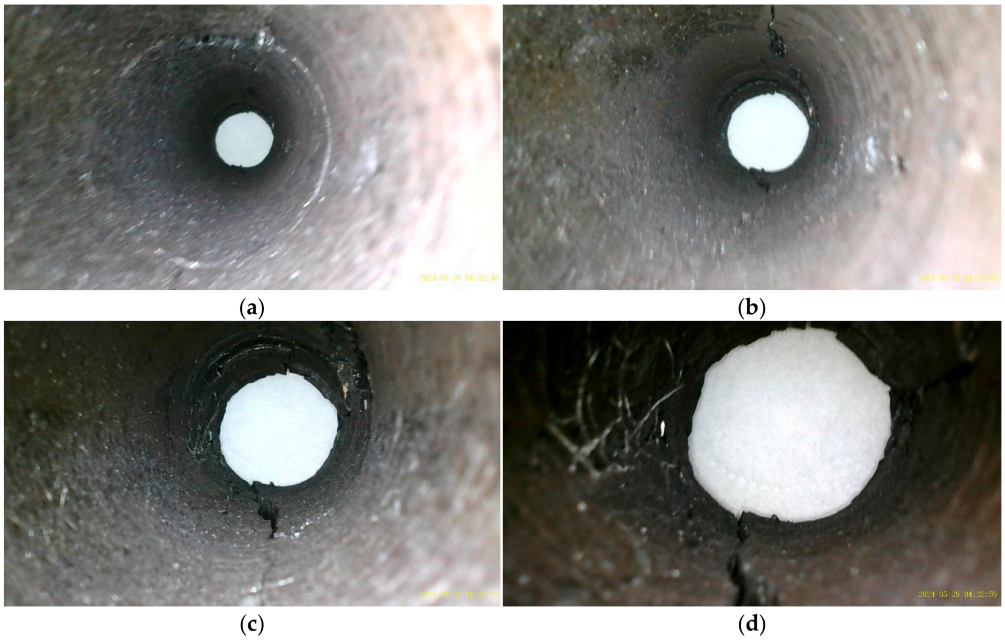


Figure 16. Endoscopic Images of Internal Fractures in Raw Coal under Loading-Unloading Conditions: (**a**) Endoscopic image 1; (**b**) Endoscopic image 2; (**c**) Endoscopic image 3; (**d**) Endoscopic image 4.

The development stage of fractures can be judged according to fracture aperture. Fractures with large apertures are generally more mature and cause more severe damage to rock mass structures, corresponding to stronger energy release and greater internal extension depth, which further directly affect the overall mechanical properties of rock mass.

Figures 17–19 sequentially illustrate the macroscopic fracture morphology, acoustic emission location results and root mean square amplitude energy nephograms of raw coal fracture under vertical loading. Figure 20 presents the borehole endoscopic monitoring images under the corresponding working condition. Combined with the engineering background of roadway excavation in this study, the fracture development characteristics in the surrounding zone of the borehole are emphatically analyzed. The observation results show that fractures originate from the borehole wall and extend radially toward the exterior of the specimen. Typical fractures include Fracture 1, Fracture 2, Fracture 5, Fracture 7 and Fracture 8. Meanwhile, acoustic emission (AE) events are basically distributed throughout the whole specimen space, and their main causes are as follows:

(1) Raw coal itself is a heterogeneous rock mass with various initial defects such as pores and micro fractures inherently existing inside. Due to the random spatial distribution of these defects, the damage initiation and propagation paths in different regions exhibit significant randomness during specimen loading, thereby forming discretely distributed AE events.

(2) The spatial distribution characteristics of AE events are affected by loading mode, loading rate, boundary constraint conditions and other factors. For instance, non uniform loading leads to heterogeneous internal stress distribution within the specimen, inducing damage at multiple positions simultaneously and triggering acoustic emission signals.

The superposition identification combining the spatial aggregation characteristics of AE events and the root mean square amplitude energy nephogram of waveforms can accurately locate the main fracture development zones and core damage regions. This method provides multi dimensional visual support for revealing the temporal spatial evolution law of coal rock fracture under excavation disturbance, and possesses important characterization value for clarifying the initiation and coalescence mechanism of fracture networks around boreholes.

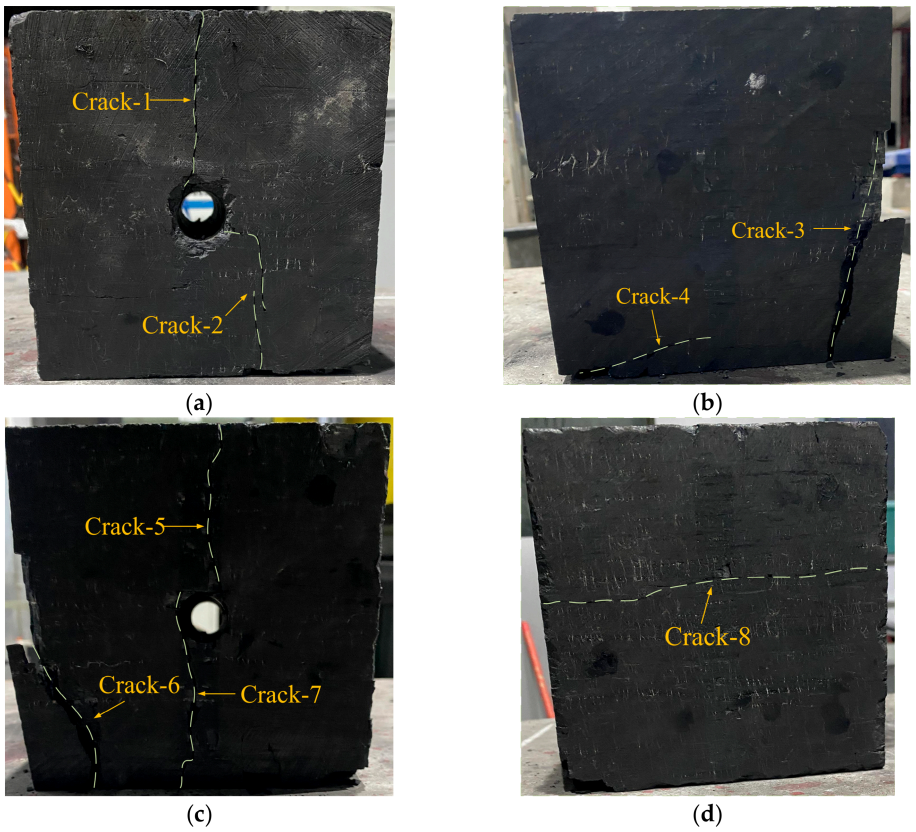


Figure 17. Macroscopic Fracture Appearance of Raw Coal under Loading Conditions: (**a**) Front view; (**b**) Right side view; (**c**) Rear view; (**d**) Left side view.

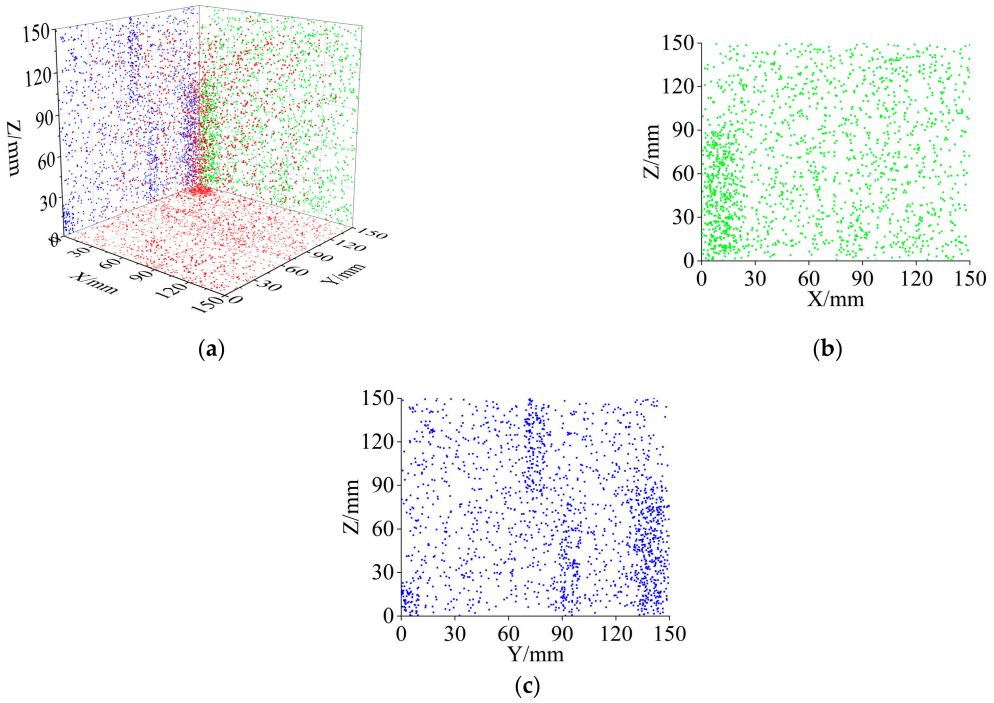


Figure 18. Location Results of Acoustic Emission Events during Raw Coal Fracture under Loading Conditions: (**a**) 3 D Acoustic Emission Location; (**b**) Location Projection on XZ Plane; (**c**) Location Projection on YZ Plane.

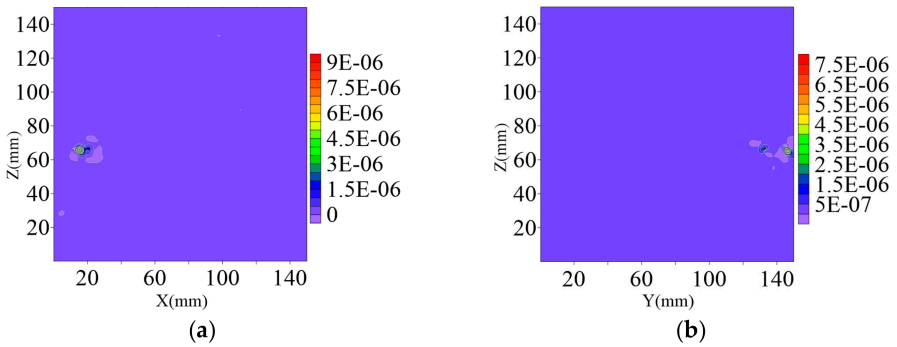


Figure 19. Acoustic Emission Nephograms of Raw Coal Fracture under Loading Conditions: (**a**) Root Mean Square Amplitude Energy Nephogram of Event Waveforms on XZ Plane; (**b**) Root Mean Square Amplitude Energy Nephogram of Event Waveforms on YZ Plane.

The spatial distribution of acoustic-emission events and energy-accumulation zones can directly indicate high-damage hazard zones around boreholes. In engineering practice, this can be used to divide surrounding-rock stability zones and optimize the layout scope and support strength of bolts and anchor cables. The joint-identification method combining spatial location and energy nephograms can effectively identify the main fracture direction, fracture coalescence paths and stress-concentration zones. It makes up for the deficiency of traditional monitoring that only reflects local deformation, and provides visual references and technical support for long-term safety monitoring of underground roadways and advance prevention-control of disaster-risk zones.

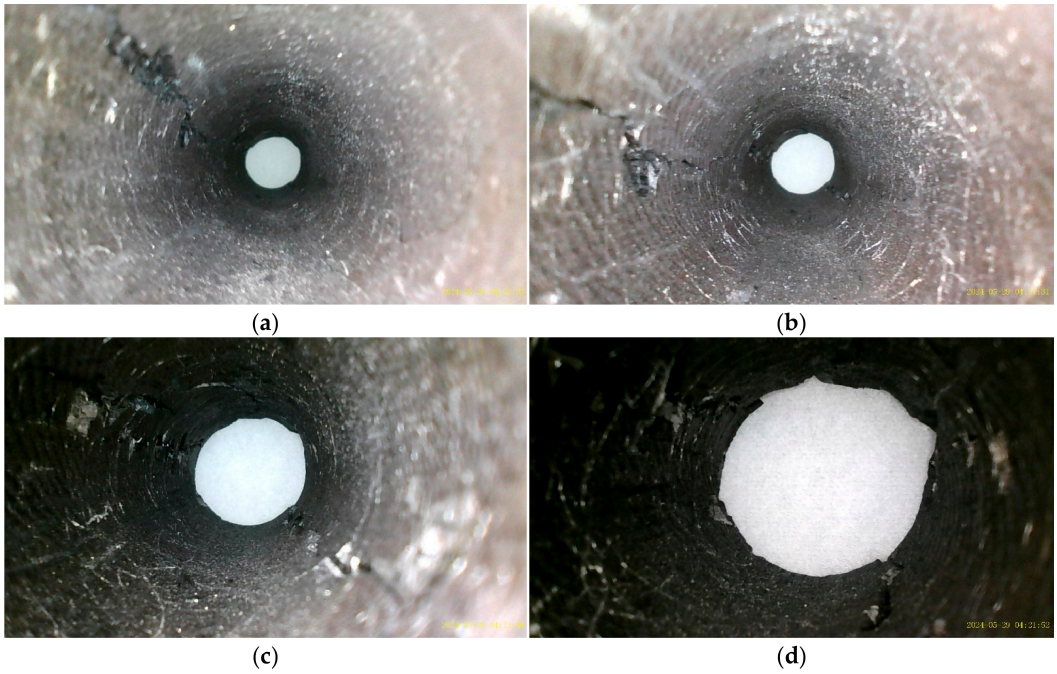


Figure 20. Endoscopic Images of Internal Fractures in Raw Coal under Loading Conditions: (**a**) Endoscopic image 1; (**b**) Endoscopic image 2; (**c**) Endoscopic image 3; (**d**) Endoscopic image 4.

The multi-parameter precursor criteria derived from acoustic-emission signals enable early identification of high-damage hazard zones around boreholes, which helps avoid over-support and facilitates the implementation of sustainable and performance-oriented support schemes for deep coal roadways. The temporal-spatial evolution rules of acoustic emission obtained in this test enrich the understanding of coal-rock dynamic disasters precursors under excavation disturbance, and can support disasters prediction and mitigation strategies for deep mining engineering.

4. Discussion

In this work, true-triaxial laboratory fracture tests were carried out on raw-coal specimens containing pre-fabricated simulated roadways under two typical stress paths: coupled vertical-loading-lateral-unloading and pure vertical loading. The temporal-spatial evolution laws of acoustic emission during coal-rock fracture were systematically obtained.

Many previous laboratory studies on coal-rock fracture have focused mainly on intact coal-rock samples under conventional triaxial compression or cyclic loading-unloading conditions, and great progress has been achieved in understanding acoustic-emission response and rock-burst precursors. Nevertheless, few experimental investigations have concentrated on raw coal with pre-excavated roadway openings subjected to the coupled stress path of vertical loading and lateral unloading, which closely reproduces the actual stress disturbance induced by deep roadway excavation. Different from intact specimens, the pre-fabricated opening produces prominent stress-concentration zones around the borehole wall, which dominate the initiation position and propagation direction of internal fractures in raw coal. As observed in our tests, fractures originate from the borehole wall and expand radially outwards, indicating that excavation-induced stress concentration is the dominant factor controlling the fracture pattern of surrounding rock of coal roadways.

Our test results reveal two distinct instability modes under different stress paths. Under the condition of vertical loading combined with lateral unloading, macroscopic instability obviously lags behind the peak value of acoustic-emission event counting, and obvious precursor information more than 150 s ahead of fracture can be captured. In con-

trast, local abrupt instability occurs under pure vertical-loading conditions without obvious abrupt change in AE event counts. This phenomenon suggests that relying merely on stress monitoring cannot reliably identify potential fracture risks for roadway surrounding rock. Multi-parameter acoustic-emission indicators, including root-mean-square amplitude energy, rectified mean value and dominant-frequency shift toward high-frequency bands, can serve as effective quantitative precursors for accelerated coal-rock fracture. Such time-frequency precursors are less affected by macroscopic deformation hysteresis and exhibit higher sensitivity for early-stage damage identification.

From the perspective of engineering application for sustainable deep mining, the spatial distribution of acoustic-emission events and high-energy accumulation zones can mark high-damage hazard regions around underground openings. This provides a feasible laboratory basis for implementing performance-oriented and sustainable support strategies. Conventional roadway support design often adopts overly conservative support parameters to prevent rock-burst disasters, which may cause material waste and increase engineering costs. Using multi-parameter AE early-warning criteria obtained in this study, high-risk zones can be identified in advance, so that targeted reinforcement measures can be implemented instead of blind over-support. This matches the core objective of sustainable geotechnical engineering: improving underground infrastructure safety while reducing material consumption and environmental footprint in deep mining.

It should be noted that the present study is based on laboratory-scale raw-coal specimens. There are inevitable gaps between indoor test conditions and complex in-situ engineering environments. Factors such as geological heterogeneity, groundwater, multiple excavation disturbances and large-scale geological structures are not reproduced in this laboratory test. In addition, only 24-channel acoustic-emission monitoring was adopted in this paper; further research is required to optimize sensor layout to improve the location accuracy for complex fracture networks. Future work will focus on combining laboratory-derived precursor criteria with field microseismic monitoring data, to promote the practical application of multi-parameter early-warning methods and further support sustainable support system design for deep coal-mine roadways.

In addition, the scale effect between laboratory specimens and in-situ engineering bodies is also an important limitation of this study, which is mainly reflected in two aspects: The raw coal specimens in laboratory tests are subjected to controlled and simplified loading conditions, with idealized stress levels, distribution patterns and boundary conditions. By contrast, the coal-rock mass at the engineering scale exists in a complex in-situ stress environment, with higher stress magnitudes and more heterogeneous stress distribution. This difference may lead to deviations in fracture propagation laws and acoustic emission response characteristics between laboratory results and field practice. The laboratory raw coal specimens have relatively high homogeneity, with limited primary fractures and structural planes. For in-situ coal-rock masses, however, multi-scale geological structures such as bedding, joints and weak planes are widely developed. These structural planes exert a more significant controlling effect on fracture evolution, energy release and disaster incubation process, which cannot be fully reproduced in laboratory-scale tests.

5. Conclusions

In this study, true triaxial loading tests and 24-channel acoustic emission (AE) monitoring were conducted on raw coal specimens with pre-fabricated simulated roadways under two stress paths: vertical loading with lateral unloading and pure vertical loading. The temporal-spatial evolution of AE during coal-rock fracture was systematically analyzed, and the control mechanisms of roadway structure and loading path on fracture patterns were clarified. The main conclusions are drawn as follows:

1. The pre-fabricated roadway induces remarkable stress concentration around the borehole. Macroscopic instability lags more than 150 s behind the AE activity peak, exhibiting clear precursor warning characteristics. Stress monitoring alone cannot reliably identify roadway fracture risk, while AE event counting serves as a valid indicator for early damage identification, providing empirical support for rock burst and dynamic disaster early warning in deep coal mines.
2. As coal rock approaches instability, AE root-mean-square amplitude energy and rectified mean value fluctuate sharply, and the dominant frequency shifts to high-frequency bands. These time-frequency parameters can be used as quantitative criteria for accelerated fracture. This analytical approach based on AE signals is free from macroscopic deformation hysteresis, and offers reference for early damage identification and dynamic support adjustment of deep roadway surrounding rock.
3. Internal fractures initiate from the borehole wall and propagate radially outward. AE events are discretely distributed across the specimen, and high-energy accumulation zones align well with major fracture zones. The combination of 3D AE location and energy nephograms accurately identifies high-damage hazard zones around roadways, compensating for limitations of traditional deformation monitoring, and provides visual support for roadway stability zoning and support parameter optimization.
4. Lateral unloading weakens confining pressure constraints and aggravates borehole stress concentration, accelerating damage development; abrupt vertical stress variation can induce local instability. The findings provide experimental and methodological support for failure mechanism analysis, disaster prevention and sustainable support design of deep high-stress roadways.

Author Contributions: Conceptualization, X.F.; methodology, Y.Z. and Q.M.; code, S.S. and S.Z.; field test and validation, Z.L. and Y.L.; data analysis, Q.M. and C.X.; writing—original draft preparation, X.F. and Q.M.; writing—review and editing, Y.Z. and W.D.; project administration, C.Z. and W.D. All authors have read and agreed to the published version of the manuscript.

Funding: Major Science and Technology Special Program of Yunnan Provincial Science and Technology Department (No. 202302AB080010).

Data Availability Statement: Dataset available on request from the authors.

Acknowledgments: We would like to thank the editor and anonymous reviewers for their constructive comments.

Conflicts of Interest: Xugang Fang, Yunpeng Zhang, Sizhan Sun, Shijian Zhang, Zhengcheng Li, Yongxiang Li, Chengtao Xin, Chaolan Zhou, and Weizhi Diao were employed by the companies Yunnan Chihong Zinc Germanium Co., Ltd. and Kunming Metallurgical Research Institute Co., Ltd. The remaining authors declare that the research was conducted in the absence of any commercial or financial relationships that could be construed as a potential conflict of interest.

References

1. Liu, J.; Xing, K.; Li, X.; Li, N.; Wang, P. Study on the Prevention and Control of Hydraulic Fracturing Impact Ground Pressure of Hard Roofs During the Initial Mining Period of Thick Coal Seam Fully Mechanized Mining Faces. *Processes* **2026**, *14*, 2113. [CrossRef]
2. Kang, H.P. Seventy years development and prospects of strata control technologies for coal mine roadways in China. *Chin. J. Rock Mech. Eng.* **2021**, *40*, 1–30. [CrossRef]
3. Wang, B.; Duan, Y.; Ren, K.; Zhang, Y. The Characteristic Strength and Damage Temporal and Spatial Evolution of the Combination Under the Coal Thickness Effect. *Processes* **2026**, *14*, 2641. [CrossRef]
4. Hu, W.; Kang, H.; Shang, Z.; Li, K.; Qiao, Z.; Chen, H. Experimental Study on Rockburst Failure Characteristics of Deeply Buried Jointed Roadway Surrounding Rock Under True Triaxial Dynamic Disturbance. *Processes* **2026**, *14*, 2513. [CrossRef]

5. Zhang, Y.P.; Ma, Q.; Du, J.H.; Chang, X.K.; Li, X.; Yan, T.; Zhang, S.J.; Yang, Z. Microseismic Early Warning Process for Mine Roof Based on Multi-Algorithm Fusion. *Process* **2026**, *14*, 1765. [CrossRef]
6. Jing, H.W.; Wu, J.Y.; Yin, Q.; Zhu, D. Experimental study on multi-source information response of force, electromagnetics and acoustics in the whole process of deformation and fracture evolution of structural surrounding rock. *Chin. J. Rock Mech. Eng.* **2023**, *42*, 1582–1598. [CrossRef]
7. Li, S.L.; Zhou, M.J.; Gao, Z.P.; Liu, X. Experimental study on acoustic emission characteristics before the peak strength of rocks under incrementally cyclic loading-unloading methods. *Chin. J. Rock Mech. Eng.* **2019**, *38*, 724–735. [CrossRef]
8. Jiang, J.J.; Deng, Z.G.; Ouyang, Z.H.; Chen, X.J. Study on acoustic emission b-value characteristics of bump-prone coal sample with different sizes. *Coal Sci. Technol.* **2019**, *47*, 120–124. [CrossRef]
9. Wang, E.Y.; Liu, X.F.; He, X.Q.; Li, X.L. Acoustic emission and electromagnetic radiation synchronized monitoring technology and early-warning application for coal and rock dynamic disaster. *J. Chin. Univ. Min. Technol.* **2018**, *47*, 942–948. [CrossRef]
10. Dou, L.M.; Feng, L.F.; Cai, W.; Li, X.W. Seismo-acoustic precursor identification and comprehensive warning model for the catastrophic failure process of coal and rock. *J. Min. Saf. Eng.* **2020**, *37*, 960–968, 976. [CrossRef]
11. Li, Z.L.; He, S.Q.; Song, D.Z.; Wang, C.W. Microseismic Temporal-Spatial Precursory Characteristics and Early Warning Method of Rockburst in Steeply Inclined and Extremely Thick Coal Seam. *Energies* **2021**, *14*, 1186. [CrossRef]
12. Wu, Z.; Pan, P.Z.; Konicek, P.; Li, S.J. Spatial and temporal microseismic evolution before rock burst in steeply dipping thick coal seams under alternating mining of adjacent coal seams. *Arab. J. Geosci.* **2021**, *14*, 2097. [CrossRef]
13. Wang, G.F.; Liu, Y.; Cao, A.Y.; Li, X.H. Rock burst energy criterion with three parameters and multi-field monitoring, early warning, and dynamic control and prevention. *J. Min. Saf. Eng.* **2021**, *38*, 895–901. [CrossRef]
14. Xie, X.B.; Li, S.Q.; Guo, J. Study on Multiple Fractal Analysis and Response Characteristics of Acoustic Emission Signals from Goaf Rock Bodies. *Sensors* **2022**, *22*, 2746. [CrossRef]
15. Majid, K.; He, X.Q.; Song, D.Z.; Li, X. Extracting and Predicting Rock Mechanical Behavior Based on Microseismic Spatio-temporal Response in an Ultra-thick Coal Seam Mine. *Rock Mech. Rock Eng.* **2023**, *56*, 3725–3754. [CrossRef]
16. Zhang, H.; Liang, L.; Lin, N.; Song, G. Microseismic comprehensive evaluation method for coal burst: A case study in the Zhaolou Coal Mine. *Sci. Rep.* **2024**, *14*, 15588. [CrossRef]
17. Ma, T.; Wang, Y.J.; Liu, N.; Zhang, S. Research on multiparameter monitoring of microseismic signals of coal and rock rupture in tunnel excavation. *Prog. Geophys.* **2024**, *39*, 818–827.
18. Jing, H.W.; Yin, Q.; Zhu, D. Experimental study on the whole process of instability and failure of anchorage structure in surrounding rock of deep-buried roadway. *J. Chin. Coal Soc.* **2020**, *45*, 889–901. [CrossRef]
19. Jing, H.W.; Zhao, Z.L.; Wu, J.Y. Disaster evolution mechanism of surrounding rock structure of deep roadway based on multi-source information representation. *J. Chin. Coal Soc.* **2023**, *48*, 176–188. [CrossRef]
20. Wu, S.C.; Hu, Z.L.; Geng, X.J.; Liu, Q. Research on Whole Process of Surrounding Rock Deformation of Diversion Tunnel Based on Full Displacement Theory. *J. Hunan Univ. (Nat. Sci.)* **2023**, *50*, 181–191. [CrossRef]
21. He, M.C.; Gong, W.L.; Zhai, H.M.; Huang, J. Physical modeling of deep ground excavation in geologically horizontal strata based on infrared thermography. *Tunn. Undergr. Space Technol.* **2010**, *25*, 366–376. [CrossRef]
22. Gong, W.L.; Wang, J.; Gong, Y.X.; Li, T. Thermography analysis of a roadway excavation experiment in 60° inclined stratified rocks. *Int. J. Rock Mech. Min. Sci.* **2013**, *60*, 134–147. [CrossRef]
23. Zhao, Y.; Lu, Y.Y.; Chen, H. A plane strain modeling study of a three-center arch for deep tunnels. *Chin. Civ. Eng. J.* **2010**, *43*, 68–74. [CrossRef]
24. Chai, J.; Wang, Z.S.; Yuan, Q. Analysis on FBG sensor detection for similar physical model deformation. *J. Xi'an Univ. Sci. Technol.* **2013**, *33*, 633–639. [CrossRef]
25. Zhu, W.S.; Zhang, Q.B.; Zhu, H.H.; Li, X.J. Large-scale geomechanical model testing of an underground cavern group in a true three-dimensional (3-D) stress state. *Can. Geotech. J.* **2010**, *47*, 935–946. [CrossRef]
26. Zhang, Y.L.; Wu, Y.P.; Li, K.F. Acoustic Emission Features of Surrounding Deformation in Experiment of Large 3D Loadable Physical Similar Simulation. *Coal Eng.* **2011**, *42*, 96–99.
27. Zhang, Y.B.; Liu, X.X.; Liang, Z.Z.; Sun, H.T. Experimental Study of Rockburst Precursor of Granite Tunnel Based on Multi-Physical Field Parameters. *Chin. J. Rock Mech. Eng.* **2014**, *33*, 1347–1357. [CrossRef]
28. Wang, Z.; Gong, X.; Cheng, Q.; Xu, Z.; Cao, Z.; Li, X. A semi-supervised approach to microseismic source localization with masked pre-training and residual convolutional autoencoder. *Appl. Sci.* **2026**, *16*, 683. [CrossRef]

Disclaimer/Publisher's Note: The statements, opinions and data contained in all publications are solely those of the individual author(s) and contributor(s) and not of MDPI and/or the editor(s). MDPI and/or the editor(s) disclaim responsibility for any injury to people or property resulting from any ideas, methods, instructions or products referred to in the content.